Effects of Mechanical Tolerances on QMF Performance for Operation in the Third Stability Zone

Thomas J. Hogan, *Member, IEEE*, and Stephen Taylor

***Abstract*—Our previously reported method of accurately simulating the performance of a quadrupole mass filter (QMF) has been applied to the investigation of the effects of electrode positional tolerance on the performance of a QMF when operated in stability zone 3 ($a \approx 3.16$ and $q \approx 3.23$). Simulations for single- and dual-electrode positional errors have been undertaken. Single-axis errors produced changes in mass peak shape that are similar to those previously reported for zone 1. Compound errors produce changes in mass peak shape that are approximately a summation of the effects obtained from individual single-axis errors. Our results show that the direction of the electrode displacement, not the electrode, is the important factor in determining the effect on QMF performance. We also show that the effects of an individual electrode radius tolerance result in changes to the mass peak shape that are similar to those produced by individual electrode positional errors. Simulations also show the suitability of unbalanced excitation voltages as a method of compensating for mechanical tolerance when operating in zone 3. From these results, we are able to provide suitable limits for the voltage accuracy and stability when employing this method of compensation.**

***Index Terms*—Mathieu stability regions, multipoles, quadrupole mass filter (QMF), tolerance, zone 3.**

I. Introduction

THE IDEAL quadrupole mass filter (QMF) would consist of four infinite hyperbolic shaped electrodes that are accurately positioned at the four corners of an imaginary square. In practice, the electrodes are finite and result in a close approximation to the ideal quadrupole electric field in the central space between the four electrodes (r_0). This electric field increases linearly with increasing displacement from the central axis and is independent in x and y. The difficulty in accurately machining, correctly mounting, and aligning hyperbolic electrodes has resulted in circular electrodes being adopted by most commercial instrument manufacturers.

A QMF constructed from circular electrodes produces an electric field that deviates further from the ideal. The resultant field can be represented as a quadrupole field plus the sum of a number of higher order fields and is termed a multipole field [1], [2]. The ratio of electrode radius r to field radius r_0, i.e., r/r_0, controls the relative magnitudes of the individual components of this multipole field [2]. Early research work identified the ratio of 1.148 [3] as producing the closest approximation to a pure quadrupole field by achieving a zero value for the dodecapole term (A_6). More recently, numerical computer simulations for operation in stability zone 1 have demonstrated that a value of r/r_0 in the range 1.120–1.130 as providing optimum performance [4]; this was later refined to 1.125 to 1.130 [5]. This value of r/r_0 has also been shown to be valid for operation in zone 3 [6]. Analytical techniques have shown that a value of 1.128–1.130 provides the optimum [2] for operation in zone 1. This was based on the influence of the sixth and tenth harmonics and ignored the effects of higher order components, which may explain the slight difference between the two findings. These findings show that the best QMF operational performance is obtained not with the closest match to the quadrupole field but where individual higher order multipole terms interact in a way that minimizes their effect most effectively [2]. We are aware of manufacturers who now use $r/r_0 = 1.127$ (the mid value) in their systems. To achieve the same performance as a hyperbolic electrode QMF, a circular electrode device requires an increase in the field radius by a factor of two, resulting in a significant increase in power (power is proportional to r_0^4) [7].

Manufacturing processes are not ideal; tolerances exist, which cause the instrument performance to deviate from the optimum. For a QMF, these manufacturing tolerances result in variations in electrode radius due to tool wear and accuracy limits of the production machinery; misalignments of the electrodes arise from the electrode mounting systems and limitations of the assembly process. In the case of longer QMFs, nonparallel alignment of the electrodes can arise due to bowing of the electrodes and/or slight differences in the mounts, all of which contribute to changes in the performance characteristics of a QMF. Additionally, the mechanical design of the instrument has to minimize any thermomechanical effects that arise from thermal cycling of the instrument during bakeout and usage.

Investigation of the effects of misaligned electrodes is extremely difficult to achieve by experiment due to the need to dismantle the QMS to change or alter the position of the electrode(s). Errors introduced due to the disassembly/reassembly cycle can introduce significant performance effects that cannot be isolated from the effects that are being investigated.

Manuscript received September 11, 2008; revised June 22, 2009; accepted June 23, 2009. Date of publication October 6, 2009; date of current version June 9, 2010. The Associate Editor coordinating the review process for this paper was Dr. Yves Rolain.

The authors are with the Department of Electrical Engineering and Electronics, University of Liverpool, Liverpool L69 3GJ, U.K. (e-mail: t.j.hogan@liverpool.ac.uk; s.taylor@liverpool.ac.uk).

Color versions of one or more of the figures in this paper are available online at http://ieeexplore.ieee.org.

Digital Object Identifier 10.1109/TIM.2009.2028221

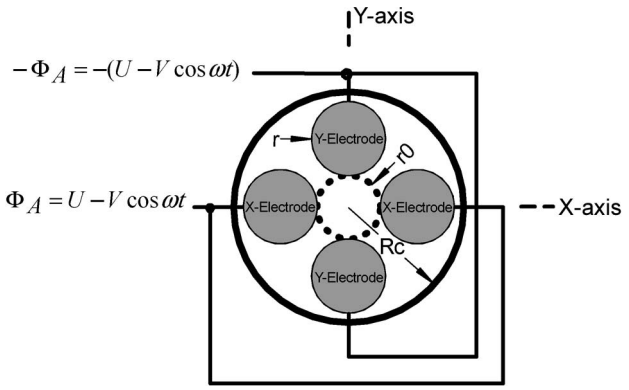

Fig. 1. End view of an optimum QMF using circular electrodes of radius r, central field radius r_0, and enclosure radius Rc, showing the combination of dc (U) and RF (V) drive voltages applied to the x- and y-axis electrodes.

Story [8], an experimentalist, produced a QMF where one electrode was movable using a jackscrew at either end of the electrode. These jackscrews passed through the vacuum enclosure enabling changes to electrode position without recourse to dismantling. Dawson [7] has reproduced some of Story's experimental results. Manufacturing a QMF for each tolerance condition is a possible alternative that would remove the errors associated with assembly and disassembly. Each unit would be a custom build, requiring closer tolerance limits than those being characterized and would incur significant costs. Numerical simulation methods overcome these experimental and cost burdens, enabling the effects of mechanical errors to be investigated and recommendations made on acceptable tolerance limits.

When one or more electrodes are displaced, the symmetry of the electrode geometry is altered. For the case of on-axis displacements, only one axis of symmetry is retained. A reduction in the degree of symmetry introduces additional multipole field terms that are not produced by an optimum QMF [1]. Previously published research has demonstrated the effects of multipole field differences on the resultant mass spectra by selective introduction of multipole field components. Examples include making the radii of the electrode pairs different to introduce an octopole field component [9], [10], shifting one of the electrode pairs further out from the axis center to introduce a number of different multipole components of similar magnitude [10], and rotational shifting of the y electrode to introduce a hexapole term [11]. These investigations used electrode displacements in excess of normal production tolerances, which resulted in multipole terms several orders of magnitude greater than those considered here.

Fig. 1 shows an end section of a QMF constructed from circular electrodes together with a definition of the drive voltages. The two x electrodes are mounted equidistant about the center on the horizontal axis and driven with the voltage Φ_A [also see (1)]. The other two electrodes, i.e., the y electrodes, are mounted equidistant about the center on the vertical axis and are driven with the voltage $-\Phi_A$. The z-axis is into and along the central axis of the QMF. The effects of electrode positional tolerance for operation in the first stability region have been recently reported [12]. Displacements of a y electrode in the y-axis greater than 0.001 r_0 resulted in degraded performance. For a displacement of an x electrode in the x-axis, changes in mass peak position occurred without any significant change in the mass peak. It was also shown that the characteristics of the resultant peaks were heavily dependent on the number of RF cycles experienced by the ions. Other factors that influenced the outcomes of positional errors were the instrument resolution setting and ion beam shape.

There is a requirement to reduce the size and power consumption of QMS instruments for space vehicle deployment and covert monitoring applications. This requirement is a driver for research into the application of microelectromechanical systems (MEMS) as a methodology for achieving these size reductions. The photolithography, oxide growth, metallization, and assembly processes associated with MEMS manufacture result in alignment and dimensional tolerances of the electrodes with a corresponding effect on performance. Devices manufactured using these techniques are more suited to rectilinear electrodes that generate an electric field inferior to circular electrodes, producing reduced performance [13].

Several versions of miniature QMFs have been reported and include the MicroQuad [14], which used a silicon structure for the mounting system with circular electrodes constructed from metallized optical fiber. Another example is the miniature QMF array, which is fabricated using silicon bulk micromachining and stainless-steel circular electrodes [15]. More recently, a complete micromachined QMF with square electrodes, including Einzel lens input optics and output optics, has been reported [16]. Experimental and simulated results show that zone 3 operation significantly improves peak shape and resolution for miniaturized mass filters when compared to zone 1 performance [15], [16].

Zone 3 also provides increased resolution and reduced mass tailing for conventional QMFs [17], [18] over that achieved with zone 1. These characteristics enable the detection of low levels of one species in the presence of high levels of an adjacent and closely spaced species [15]. Zone 3 also provides improved immunity to variations in the r/r_0 ratio of circular electrodes [6]. Better understanding of the impact of electrode positional tolerance on QMF performance when operating in stability zone 3 was seen as a prerequisite to its greater usage. This was the motivation for undertaking this work.

II. Theory

Consider the QMF shown in Fig. 1, where Φ_A is defined as follows:

$$\Phi_A = U - V\cos\omega t. \tag{1}$$

Here, U is the applied dc voltage, V is the zero-to-peak ac (RF) voltage, ω is the angular frequency of voltage V, and t represents time. This electrode and drive voltage configuration results in a multipole voltage distribution in the central field, which can be represented by [1], [2]

$$\Phi(x,y) = \Phi_A \sum_{N=0}^{\infty} \frac{A_N \Phi_N}{r_o^N} \tag{2}$$

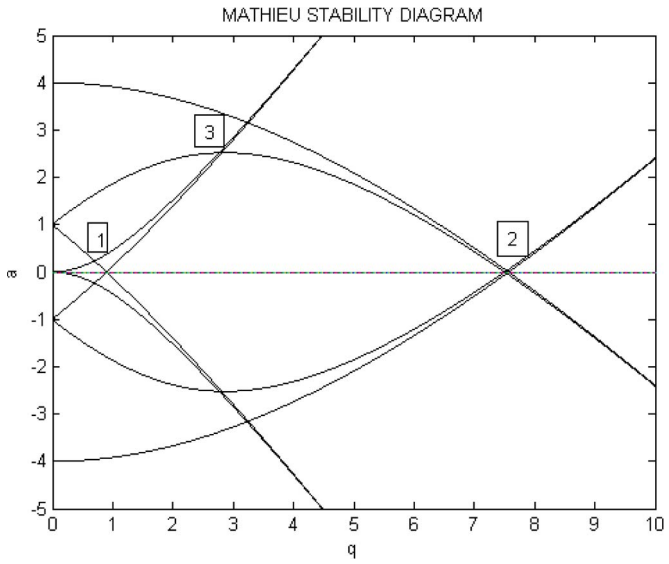

Fig. 2. Mathieu stability diagram showing the first three stability regions.

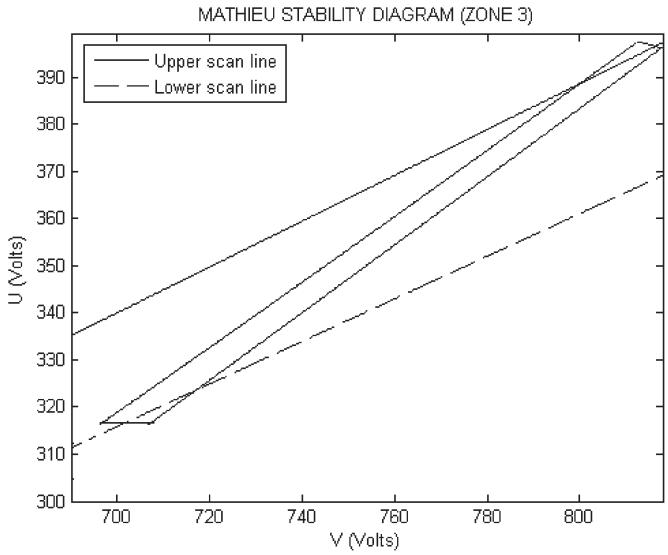

Fig. 3. Zone 3 stability diagram in $U-V$ space showing upper and lower scan lines for Ar^+ ion species $(m/z = 40)$ for the test conditions in Table I.

where A_N is the amplitude of the multipole Φ_N consisting of $2N$ poles, with $A_0\Phi_0$ defining the offset potential, $A_1\Phi_1$ defining the dipole potential, $A_2\Phi_2$ defining the quadrupole potential, $A_3\Phi_3$ defining the hexapole potential, and continuing thereon.

The electrode and drive voltage configuration of Fig. 1 has two axis of symmetry and two of antisymmetry, and only multipole terms in which $N = 4n + 2$, $n = 0, 1, 2, 3, \ldots$, contribute to the field. For electrode configurations where electrodes are displaced or of different radii, the degree of symmetry is reduced. These geometrical imperfections will result in additional multipole terms being introduced and variations in their amplitudes [1].

Assuming that the geometry is consistent throughout the length of the QMF and ignoring fringing fields, a 2-D field model can be used. One further assumption is made, i.e., the x and y fields are uncoupled; this is valid if small incremental movements of the ion are considered. With these assumptions, the motion of ions can be calculated using Newton's second law of motion and the electric field at the ion position (x, y) and results in

$$m\frac{d^2x}{dt^2} = -e\frac{\partial\Phi_{(x,y)}}{\partial x} \tag{3}$$

$$m\frac{d^2y}{dt^2} = -e\frac{\partial\Phi_{(x,y)}}{\partial y} \tag{4}$$

where m is the mass of the ion, and e is the charge on the ion.

Only certain combinations of voltages result in an ion having the possibility of a stable trajectory through a QMF. For hyperbolic electrodes, solutions of the Mathieu equations provide a method of determining these voltages [19]. This method also provides an approximate indication of the behavior of an optimum circular electrode QMF. A Mathieu stability diagram (Fig. 2) provides a graphical representation of the solutions of these equations that occur where the bounded areas overlap. The Mathieu diagram is symmetrical about the a_u axis [20], [21], and in Fig. 2, the y-stability region has been reflected from the third to the second quadrant for clarity. As a further and more usual simplification, Fig. 3 has been restricted to the first quadrant.

Transformation of the $a-q$ space diagram into a $U-V$ space stability diagram can be achieved by use of the following equations:

$$a_x = -a_y = \frac{8eU}{m\omega^2 r_0^2} \tag{5}$$

$$q_x = -q_y = \frac{4eV}{m\omega^2 r_0^2} \tag{6}$$

where a_x, a_y, q_x, and q_y are the Mathieu parameters, and the remaining symbols are as previously specified.

A $U-V$ space representation of stability zone 3 is shown in Fig. 3. This is of approximately a rectangular shape, and two corners are suitable for creating mass filtering action, the lower right corner at $a \approx 2.52$ and $q \approx 2.82$ and the upper left corner at $a \approx 3.16$ and $q \approx 3.23$. For all our simulations, we have used the upper left corner of this stability zone.

III. Simulation Techniques

We have used the same software configuration as previously reported [6], which consists of Poisson/Superfish [22] and QMS2D-Field [6]. Poisson/Superfish is a public access suite of programs for solving a range of magnetostatic problems. It was originally written by R. F. Holsinger in collaboration with K. Halbach for particle accelerator design. At present, they are maintained by the Los Alamos National Laboratory (LANL) who provide a download website for the software [23]. The following three modules from the Poisson/Superfish suite were used for this work: 1) Automesh; 2) Poisson; and 3) SF7. Automesh enables the problem geometry, material electrical characteristics, electrode voltages, and meshing grid pitch to be defined in a text file. Geometric models were created for a range of electrode displacements and electrode radii. Automesh

TABLE I
COMPUTER SIMULATION TEST CONDITIONS

QMF PARAMETER	CONDITION
Length	254 mm
r_0	2.76 mm
r/r_0	1.127
Frequency	2 MHz
Detector radius	2.76 mm
Housing radius	$3.6r_0$
Ion Source	
Ion energy	50 eV
Ion source radius	0.5 mm
Ion energy spread	0
Ion angular spread	0
Operating point	
a	3.16
q	3.23
Ion species	40 m/z

divides the space between electrodes and the problem boundary (the circular enclosure forms the problem boundary) into a 2-D triangular mesh. The resultant output is a binary solution file that provides the problem definition input to Poisson. Poisson uses a successive overrelaxation algorithm to solve the field and rewrites the binary solution file with the resultant field data. It also provides the multipole coefficients in a secondary file. Finally, SF7, the field interpolator program processes the field data to produce a user-defined rectangular grid of 1600 by 1600 electric field values for the central space between the four electrodes.

QMS2D-Field is a custom in-house software package providing facilities to set the operating and physical characteristics of the QMF, generate the entry conditions for a large number of ions, and calculate the trajectories of these ions. A utility program FieldCalc was used to extract and format field data from the SF7 generated field file into a form compatible with our software.

For each electrode arrangement, mass spectra were generated using a minimum of 10^5 ions and 500 increments across the mass range shown in the figures. An instrument resolution control η (0%–100%) is used to vary the resolution setting of the instrument [see (7)], with $\eta = 100\%$, representing the peak of the upper left corner of the zone 3 stability region ($a_{\text{tip}} = 3.16,\ q_{\text{tip}} = 3.23$). The remainder of the test conditions are shown in Table I, unless otherwise stated. We have

$$U = \eta \frac{V a_{\text{tip}}}{2 q_{\text{tip}}}. \tag{7}$$

A low-amplitude structure is visible on the mass peaks, which is due to minor changes in the acceptance of the QMF as the mass scan position changes. The entry conditions of a significant number of ions are close to the acceptance boundary, and these result in slight variations in transmission as the mass scan is incremented. Significantly increasing the number of ions simulated at each mass step would reduce this variation but would increase the overall simulation time. Alternatively, digital filtering could be applied to smooth the mass peak without loss of key information.

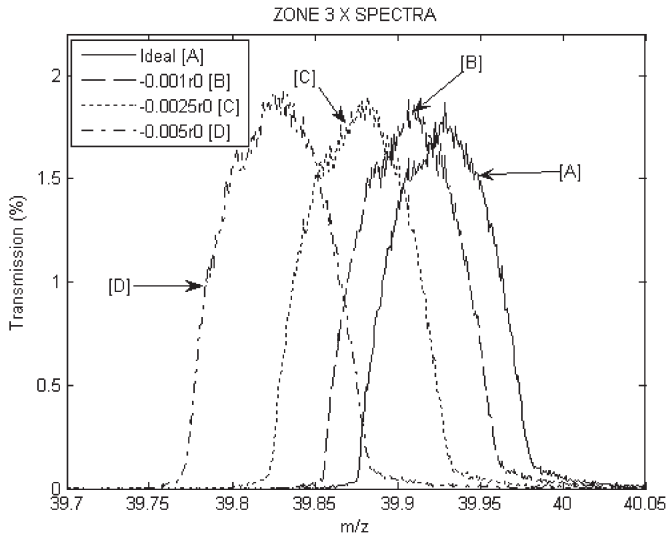

Fig. 4. Simulated mass spectra for Ar^+ ion species $(m/z = 40)$ for a range of inward radial displacements of a single x electrode.

TABLE II
MASS SPECTRA CHARACTERISTICS FOR A RANGE OF RADIAL INWARD DISPLACEMENTS (NEGATIVE) FOR x AND y ELECTRODES

Displaced Electrode	Parameter	Displacement (on-axis)			
		0	**-0.001r_0**	**-0.0025r_0**	**-0.005r_0**
X	**Peak position (amu)**	39.93	39.909	39.88	39.82
	Peak height (%)	1.79	1.83	1.86	1.89
	Resolution 50% PH	524	514	497	476
	Resolution 10% PH	394	388	378	369
Y	**Peak position (amu)**	39.93	39.904	39.89[a]	39.84[a]
	Peak height (%)	1.79	1.38	0.65[a]	0.33[a]
	Resolution 50% PH	524	544	595[a]	937[a]
	Resolution 10% PH	394	368	301[a]	248[a]

(Note[a] main peak value, PH = peak height).

IV. ELECTRODE POSITIONAL TOLERANCE

Effects of an inward radial displacement of single x and y electrodes were investigated for a range of displacements up to $0.005r_0$, at which point an isolated satellite peak is identifiable. Fig. 4 shows the result of increasing the inward radial displacement of an x electrode. We can observe that an increasing displacement produces an increasing shift of the mass peak to a lower mass position. From inspection of the data in Table II, we can see that the incremental mass peak shift is approximately proportional to the incremental electrode displacement. Along with this shift is a decrease in resolution and an increase in peak height (sensitivity) for an increasing inward displacement. The shift on the mass scale is correctable through calibration. As the sensitivity increases with increased displacement, it may be possible to increase the instrument resolution (η) to compensate for the reduction in resolution, without the sensitivity decreasing below that of the optimum QMF. Slight changes to the structure of the noise on each of the mass peaks are observable, but no significant change in the low and high mass tails occur.

A radial inward displacement of a single y-axis electrode produces significant changes to the mass spectra, as can be seen in Fig. 5. An increasing inward displacement of a y electrode

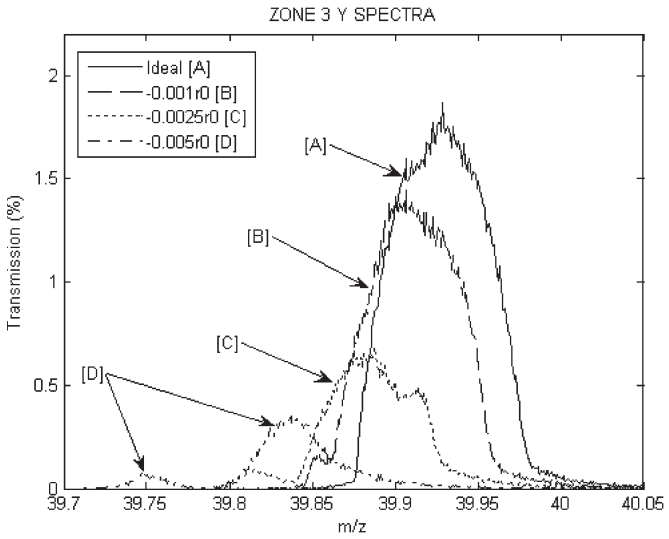

Fig. 5. Simulated mass spectra for Ar^+ ion species ($m/z = 40$) for a range of inward radial displacements of a single y electrode.

produces a proportional shift of the mass peak to a lower mass value. This shift is slightly greater than the shift produced by the equivalent x-electrode displacement. Decreasing peak height and a reduction in the steepness of the edges are observable as the y displacement increases. For small y displacements, a shoulder emerges on the low mass side of the mass peak. The higher mass side of this shoulder decreases in amplitude, while the opposite end increases in amplitude with increasing y displacement. At the extremes of the displacement range, the shoulder separates from the main peak, forming a satellite peak. On the high mass side of the peak, a secondary peak appears and disappears finishing with the formation of a concave edge at the limits of the displacement. Outward displacements of the x and y electrodes result in very similar changes to those obtained for inward displacements of x and y electrodes, except that the mass peak shifts are to a higher mass position.

When one or more electrodes are displaced, the symmetry of the electrode geometry is altered. This reduction in the degree of symmetry introduces into the field the $4N$ multipole terms that are not present in the optimum QMF field [1], [2]. Table III contains the multipole coefficients for the range of electrode displacements investigated. For the optimum circular electrode geometry, only the A_2, A_6, A_{10}, and A_{14} terms are present. We will first examine the changes to these components. The A_2 multipole coefficient increases with increasing electrode displacement for both x- and y-electrode displacements. We also observed a comparable decrease in this term for outward on-axis displacements. This increase/decrease in A_2 has an equivalent effect to an increase/decrease in Φ_A and is the major contributor to the observable shift on the mass scale. Considering next the remaining $4N + 2$ multipole terms A_6, A_{10}, and A_{14}, our results show that these vary by a very small amount. Previous research has shown that these terms depend on the r/r_0 ratio and that, possibly, A_6 and A_{10} act in a way to self compensate [2]. As these three terms do not vary significantly, we can assume that they do not contribute in any major way to the effects that are observed. Examination of Table III shows that for these displacements, the A_4, A_8, and A_{12} multipole ($4N$ terms) are present, and all are of the same sign and increase with increasing displacement. The magnitude of the A_4 and A_8 terms are approximately two orders of magnitude less than A_6 and A_{10} and an order of magnitude greater than the A_{12} term. The presence of the A_4, A_8, and A_{12} terms result in the shoulder forming and for the satellite appearing when the y electrode is displaced. It is not possible to deduce from our results the exact contribution that each of these terms make to the overall effect. It may well be the case that the three terms reinforce each other to achieve the overall effect, or more likely, given the nonlinear nature of these coupled terms, they interact in a more complex manner.

The results show that the effect of changes due to electrode displacement are not the same for x and y electrodes. Although the optimum electrode geometry is symmetrical about the x- and y-axes, there is asymmetry due to the average (mean) potential that is applied to the electrodes and the charge on the ion. The mean potential averaged over a number of cycles is negative for the y electrodes and positive for the x electrodes. Due to the positive charge on the ions, they will be, on the average, repelled by the x electrodes and attracted to the y electrodes. This results in an increased instability of the ions in the y-axis with a distortion of the low mass side of the y stability region. These observed effects on peak shape are due to a combination of the A_4, A_8, and A_{12} multipole terms and the average polarity of the electrode potential. This interrelationship between the effects of electrode displacement and electrode potential has been previously reported [9]. The relationship is also confirmed by the industry practice of exchanging the voltage drive to the x and y electrodes as a method of improving QMF performance.

Differences in the radius of an electrode can occur due to mechanical tolerances of the manufacturing process and can result in electrodes of different radii being present in a QMF assembly. Simulations undertaken for a single electrode of differing radius, with all the electrodes mounted on a common pitch center, resulted in mass peak changes similar to those obtained with electrode displacement. Increasing the electrode radius resulted in mass peak changes corresponding to an inward electrode displacement, and decreasing the electrode radius produces results similar to those for an outward electrode displacement.

Fig. 6 shows the effects of compound misalignments, where both x and y electrodes are displaced. The resultant mass peak shapes are similar in character to those obtained for a y-only inward displacement. However, there are differences that are worth noting. Table IV shows that when the x and y electrodes both have inward radial displacements, the peak position shift is greater. It is approximately equivalent to the sum of the individual shifts obtained for x and y displacements. The satellite peak moves slightly closer to the main peak, the peak heights are marginally greater, and there is increased noise on the main peak. An inward displacement of a y electrode coupled with an outward displacement of an x electrode results in the main peak being close to the optimum position. The relative peak positions of the main and satellite peak stay the same with a decrease in their peak heights. These effects demonstrate that the electrode tolerances of individual electrodes can self

TABLE III
MULTIPOLE COEFFICIENTS OBTAINED USING POISSON FOR ON-AXIS DISPLACEMENTS OF x AND y ELECTRODES

Multipoles / Displacement	A_2	A_4	A_6	A_8	A_{10}	A_{12}	A_{14}
0	1.0016E+00	-	1.20E-03	-	-2.43E-03	-	-2.96E-04
-0.001r_0	1.0021E+00	1.58E-05	1.18E-03	1.17E-05	-2.43E-03	1.90E-06	-2.97E-04
-0.0025r_0	1.0029E+00	3.98E-05	1.16E-03	2.96E-05	-2.44E-03	4.79E-06	-2.98E-04
-0.005r_0	1.0042E+00	8.10E-05	1.11E-03	5.99E-05	-2.46E-03	9.69E-06	-3.00E-04

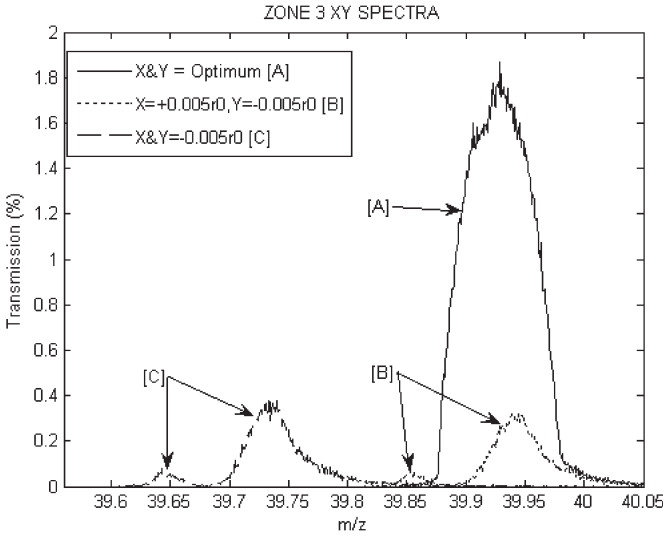

Fig. 6. Simulated mass spectra for Ar^+ ion species $(m/z = 40)$ for a range of compound inward radial displacements of an x and a y electrode.

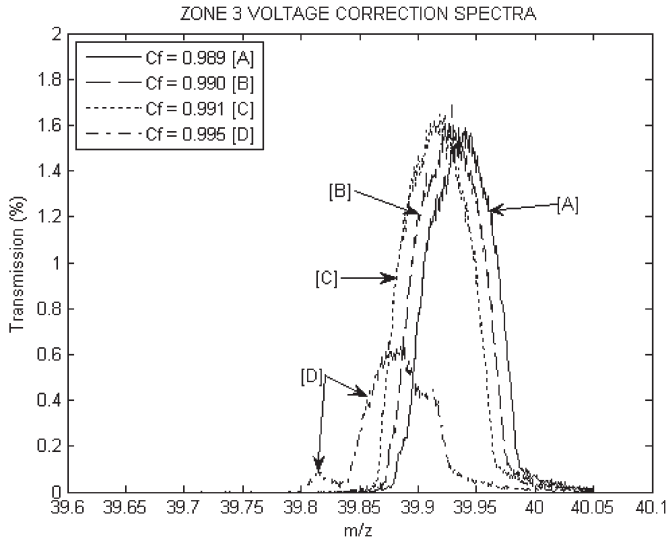

Fig. 7. Simulated mass spectra for Ar^+ ion species $(m/z = 40)$ for a 0.005 r_0 inward radial displacement of a y electrode for a range of compensation factors (C_f). A voltage $C_f(-U + V\cos\omega t)$ is applied to the displaced y electrode. (See Fig. 6 for a comparison with the optimum mass spectra.)

TABLE IV
MASS SPECTRA CHARACTERISTICS FOR COMPOUND RADIAL DISPLACEMENTS OF AN x AND A y ELECTRODE

Parameter	Displacement (on-axis)		
	x = 0 y = 0	**x = +0.005r_0 y = -0.005r_0**	**x = -0.005r_0 y = -0.005r_0**
Peak position (amu)	39.93	39.95	39.74
Peak height (%)	1.79	0.31[a]	0.36[a]
Res 50% PH	524	907[a]	968[a]
Res 10% PH	394	391[a]	358[a]

(Note[a] main peak value).

compensate for the quadrupole term, but the effects of the higher order field components on peak shape are only marginally altered.

Modification of the drive voltage on the displaced electrode is a method of compensation that has previously been reported for zone 1 operation [12] and is the subject of a number of patents [24]–[26]. For an inward or outward displacement of an electrode, changes to the multipole components of the field will occur. Decreasing or increasing the drive voltage to the displaced electrode(s) provides a method of compensating for these electrode displacements. Simulated mass peaks when employing this compensation method for operation in stability zone 3 are shown in Fig. 7. Comparing this figure to the uncorrected mass peak in Fig. 4 shows that decreasing the electrode drive voltage alters the mass peak, and with $C_f = 0.990$ [where the applied voltage is $C_f(-U + V\cos\omega t)$], a close match to the optimum is obtained. This confirms the previously reported correction factor of twice the displacement error [12] and demonstrates that the electric field is defined by the electrode geometry, relative magnitude, and sign of the electrode voltages. It is therefore possible when considering the overall QMS system that a tradeoff between mechanical accuracy and electrode drive system complexity can be made. An important consideration when employing this method of correction is the stability and accuracy of the drive voltages as a deviation in the relative y electrode drive voltage will cause the mass peak to degrade in a similar fashion that would be produced by a displaced electrode. From our simulations, we consider that the total error budget for the drive voltage should not be greater than $\pm 0.1\%$.

Fig. 8 shows the results of mounting errors that produce orthogonal shifts of an electrode with respect to its reference axis. For an x electrode with a displacement in the y-axis, distortions to the mass peak were observable, together with the emergence of a satellite peak at the extremes of the displacement. In this case, no significant shift in the peak position was observable. For the case of a y-axis electrode shifted in the x-direction, very little variation of the mass peak or position was observable.

Using the technique described previously, Fig. 9 shows the effect of compensating for y displacements of an x electrode by applying the correcting voltage to one of the y electrodes. The compensating voltage is applied to the upper electrode for positive y displacements and the lower electrode for negative y displacements. This compensation restores the mass peak shape and is accompanied by a marginal reduction in peak height and a shift to a higher mass position for both types

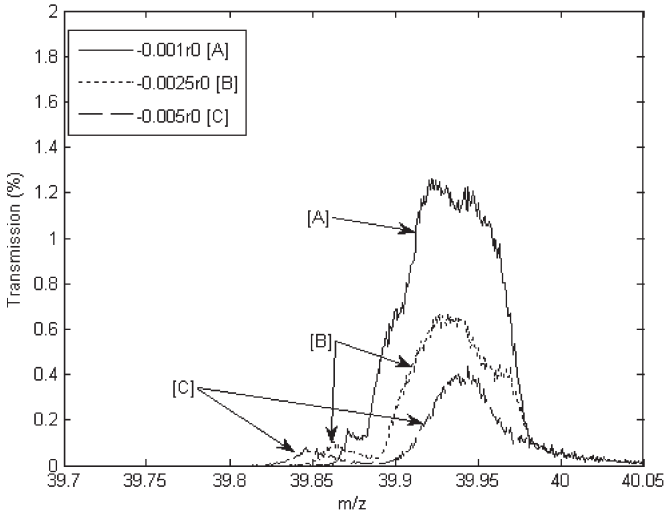

Fig. 8. Simulated mass spectra for Ar^+ ion species $(m/z = 40)$ for a range of y-axis displacements of an x electrode. (For a comparison with the optimum performance, see Fig. 6.)

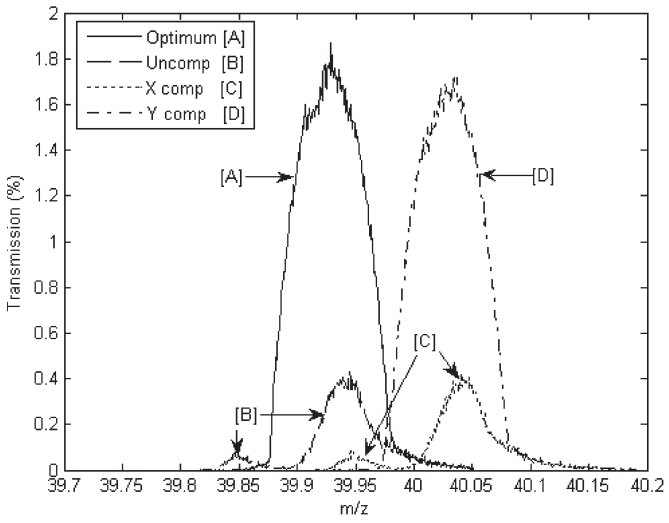

Fig. 9. Simulated mass spectra for Ar^+ ion species $(m/z = 40)$ for a displaced x electrode shifted by $0.005r_0$ in the y-axis, showing the effects of compensation $(C_f = 0.990)$ applied to the x and y electrodes individually.

of displacement. Application of the correcting voltage to the misplaced x electrode results in a shift in the mass peak but with no accompanying correction to the mass peak shape.

The number of RF cycles that the ions experience determines the quality of the mass peak [7], [27]. For zone 1 operation, this relationship is also true when the electrodes are displaced [12]. Fig. 10 shows this relationship for zone 3. At 1 MHz (with the lowest number of cycles), the main peak is very wide, not decaying to the 0.1% transmission value within the range of the graph. The satellite is apparent with the satellite to main peak valley greatly raised above the baseline. As the frequency is increased (in which the number of cycles to which the ion is exposed also increases), the relative height of the satellite decreases more rapidly than the main peak with a defined base line separation appearing. Above 4 MHz (corresponding to 65 cycles), the incremental changes are much smaller, and above 8 MHz (130 cycles), no discernible difference can be

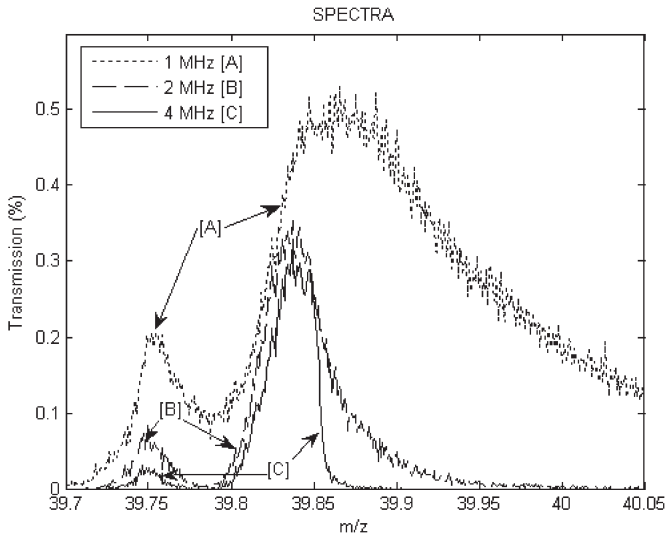

Fig. 10. Simulated mass spectra for Ar^+ ion species $(m/z = 40)$ for a $0.005r_0$ inward radial displacement of a y electrode for a range of RF drive frequencies.

detected with increasing frequency. This limiting condition occurs at a much lower value than for zone 1.

V. Conclusion

We have used our previously reported custom and public domain software to understand the effects on performance of both mechanical and electrical tolerances within a QMS mass filter system when operating in stability zone 3.

These results have demonstrated that both electrode positional and dimensional tolerances have a major impact on the ultimate performance of a QMF. Minor radial positional errors, together with small changes in the radius of a single y electrode, produce significant changes to the shape of the mass peak. At the extremes of the manufacturing tolerances examined, the appearance of a satellite peak on the low mass side is observed. At their extremes, these effects would greatly influence the ability to discriminate between close adjacent peaks. The effect of mechanical tolerances on the x electrode is not as severe, resulting only in shifts in the mass peak and minor changes to peak height. A suitable calibration procedure will allow for correction of any mass scale shift. For orthogonal displacements of an electrode, similar effects to those already described arise but associated with the opposite axis electrode. A y-axis shift of an x electrode produces similar peak shape changes as those experienced for a y-axis shift of a y electrode for the same magnitude of displacement. For an x-axis shift of a y electrode, there are only marginal peak changes. This indicates that the critical issue is the axis of the displacement and not the actual electrode affected. We have also demonstrated that mechanical tolerance effects are cumulative, and that because of this, tolerances must be specified for the instrument as a whole and not for individual electrodes.

Our results also demonstrate that the previously reported method of compensation for a displaced electrode by adjusting the electrode drive voltages is also valid for a QMF operated in zone 3 and for orthogonal shifts. As this method

of compensation can introduce peak shape errors similar in character to displaced electrodes, it is necessary to maintain tight control of the differential voltages.

REFERENCES

[1] M. Szilagyi, "Determination of electric and magnetic fields," in *Electron and Ion Optics*, I. Brodie and J. J. Muray, Eds. New York: Plenum, 1988.

[2] D. J. Douglas and N. V. Konenkov, "Influence of the 6th and 10th spatial harmonic on the peak shape of a quadrupole mass filter with round rods," *Rapid Commun. Mass Spectrom.*, vol. 16, no. 15, pp. 1425–1431, 2002.

[3] I. E. Dayton, F. C. Shoemaker, and R. F. Mozley, "The measurement of two-dimensional fields—Part 2: Study of a quadrupole magnet," *Rev. Sci. Instrum.*, vol. 25, no. 5, pp. 485–489, May 1954.

[4] J. R. Gibson and S. Taylor, "Numerical investigation of the effect of electrode size on the behaviour of quadrupole mass filters," *Rapid Commun. Mass Spectrom.*, vol. 15, no. 20, pp. 1960–1964, 2001.

[5] J. R. Gibson and S. Taylor, "Asymmetrical features of mass spectral peaks produced by quadrupole mass filters," *Rapid Commun. Mass Spectrom.*, vol. 17, no. 10, pp. 1051–1055, 2003.

[6] T. J. Hogan and S. Taylor, "Performance simulation of a quadrupole mass filter operating in the first and third stability zones," *IEEE Trans. Instrum. Meas.*, vol. 57, no. 3, pp. 498–508, Mar. 2008.

[7] P. H. Dawson, "The mass filter: design and performance," in *Quadrupole Mass Spectrometry and its Applications*. Amsterdam, The Netherlands: Elsevier, 1976, pp. 125–127. (Reprinted as an "American Vacuum Society Classic" by the American Institute of Physics under ISBN 1-56396-455-4), Holland.

[8] M. S. Story, paper presented at the Pacific Conference on Chemistry and Spectroscopy, Anaheim, CA, Oct. 6–9, 1969.

[9] C. Ding, N. V. Konenkov, and D. J. Douglas, "Quadrupole mass filters with octopole fields," *Rapid Commun. Mass Spectrom.*, vol. 17, no. 22, pp. 2495–2502, 2003.

[10] M. Sudakov and D. J. Douglas, "Linear quadrupoles with added octopole fields," *Rapid Commun. Mass Spectrom.*, vol. 17, no. 20, pp. 2290–2294, 2003.

[11] N. V. Konenkov, F. Londry, C. Ding, and D. J. Douglas, "Linear quadrupole mass with added hexapole fields," *Rapid Commun. Mass Spectrom.*, vol. 17, no. 22, pp. 2495–2502, Nov. 2003.

[12] S. Taylor and J. Gibson, "Prediction of the effects of the imperfect construction of a QMS filter," *J. Mass Spectrom.*, vol. 43, no. 5, pp. 609–616, May 2008.

[13] T. J. Hogan, S. Taylor, K. Cheung, L. Velasquez-García, and A. I. Akinwande, "Simulation of a square electrode MEMS quadrupole mass filter operating in stability zones 1 and 3," in *Proc. 56th ASMS Conf. Mass Spectrom. Allied Topics*, Denver, CO, Jun. 1–5, 2008.

[14] S. Taylor, B. Srigengan, J. R. Gibson, D. Tindall, R. Syms, T. Tate, and M. Ahmed, "A miniature mass spectrometer for chemical and biological sensing," in *Proc. SPIE Int. Soc. Opt. Eng.*, 2000, vol. 4036, pp. 187–193.

[15] L. Lebel, L. F. Velasquez-García, and A. I. Akinwande, "Arrays of microfabricated quadrupole mass filters," in *Tech. Dig. 18th Int. Vac. Nanoelectron. Conf.*, Jul. 10–14, 2005, pp. 366–367.

[16] K. Cheung, L. F. Velásquez-García, and A. I. Akinwande, "Fully batch-fabricated linear quadrupole mass filters," in *Proc. IEEE Int. Conf. Solid-State Sens., Actuators, Microsyst.*, Hilton Head Island, SC, 2008, pp. 316–319.

[17] S. Hiroki, T. Ebe, and Y. Murakami, "Separation of helium and deuterium peaks with a quadrupole mass spectrometer by using the second stability zone in the Mathieu diagram," *Rev. Sci. Instrum.*, vol. 63, no. 8, pp. 3874–3876, Aug. 1992.

[18] C. Day, "The use of a high-resolution quadrupole gas mass spectrometer system for selective detection of helium and deuterium," *Vacuum*, vol. 51, no. 1, pp. 21–30, Sep. 1998.

[19] P. H. Dawson, "Principles of operation," in *Quadrupole Mass Spectrometry and its Applications*. Amsterdam, The Netherlands: Elsevier, 1976, pp. 9–64. (Reprinted as an "American Vacuum Society Classic" by the American Institute of Physics under ISBN 1-56396-455-4), Holland.

[20] N. W. McLachlan, "Calculation of characteristic numbers and coefficients," in *Theory and Application of Mathieu Functions*. Oxford, U.K.: Oxford Univ. Press, 1951. Reprinted.

[21] R. E. March and J. F. J. Todd, "Theory of quadrupole instruments," in *Quadrupole Ion Trap Mass Spectrometry*, J. D. Winefordner. Ed., 2nd ed. Hoboken, NJ: Wiley-Interscience, 2005.

[22] F. L. Krawczyk, J. H. Billen, R. D. Ryne, H. Takeda, and L. M. Young, "The Los Alamos accelerator code group," in *Proc. IEEE Particle Accelerator Conf.*, 1995, vol. 4, pp. 2306–2308.

[23] Poisson/Superfish, LANL. [Online]. Available http://laacg1.lanl.gov/laacg/services/download_sf.phtml

[24] D. M. Burns, S. Taylor, and J. R. Gibson, "Quadrupole mass filter," U.K. Patent GB2 390 222, Jul. 31, 2003.

[25] D. M. Burns, S. Taylor, and J. R. Gibson, "Quadrupole mass filter," U.S. Patent 6 940 068, Sep. 6, 2005.

[26] D. M. Burns, S. Taylor, and J. R. Gibson, "Quadrupole mass filter," European Patent EP1 649 488, Apr. 26, 2006.

[27] F. M. Ma and S. Taylor, "Simulation of ion trajectories through the mass filter of a quadrupole mass spectrometer," *Proc. Inst. Elect. Eng.—Sci. Meas. Technol.*, vol. 143, no. 1, pp. 71–76, Jan. 1996.

Thomas J. Hogan (M'09) obtained the qualifications for Chartered Engineer (electrical and electronic) in 1971 from Hendon College of Technology (now Middlesex University), London, U.K., and received the M.Sc. degree in microelectronics (with distinction) from the University of Bolton, Bolton, U.K., and the University of Northumbria, Newcastle, U.K., in 2004. He is currently an external student with the Department of Electrical Engineering and Electronics, University of Liverpool, Liverpool, U.K.

He is an independent consultant engineer in Cambridge, U.K., and has acted for organizations such as the DTI, BAe, and Thales on the design of bespoke electronic and software systems, including computer graphics, satellite imaging, scientific instrumentation, and laser systems. His professional interests include instrumentation, automotive, and embedded control. His research interests include numerical simulation, instrumentation, and reversible computing.

Mr. Hogan is a European Engineer and a member of the Institute of Engineering and Technology, U.K.

Stephen Taylor received the B.Sc. degree from Imperial College, London, U.K., in 1978, and the M.Eng. and Ph.D. degrees from the University of Liverpool, Liverpool, U.K., in 1983 and 1988, respectively.

He is currently a Reader with the Department of Electrical Engineering and Electronics, University of Liverpool, where he teaches electromagnetics and MEMS design. He has acted as a consultant to several U.K. companies and is the Director of a university spinout company. He is a Guest Editor for the *Journal of American Society for Mass Spectrometry*. He is the author or coauthor of over 200 articles, patents, or publications in the open scientific literature. In 1995, he invented and codeveloped the (then) world's smallest mass spectrometer and the first to be microengineered in silicon.

Dr. Taylor is a Chartered Engineer, a Fellow of the Institute of Engineering and Technology, and a Fellow of the Electrical Research Association. He is a member of the Organizing Committee for the RGA Users Group and a member of the Program Committee for the Harsh Environment Mass Spectrometry Conference.